Nano Energy 61 (2019) 259–266

Contents lists available at ScienceDirect

Nano Energy

journal homepage: www.elsevier.com/locate/nanoen

Full paper

A planar supercapacitor made of supramolecular nanofibre based solid electrolyte exhibiting 8 V window

Suman Kundu[a,b,1], Umesha Mogera[a,1], Subi J. George[c], Giridhar U. Kulkarni[a,*]

[a] Centre for Nano and Soft Matter Sciences, Jalahalli, Bangalore, 560013, India
[b] Manipal Academy of Higher Education, Manipal, Karnataka, 576104, India
[c] Supramolecular Chemistry Laboratory, New Chemistry Unit, Jawaharlal Nehru Centre for Advanced Scientific Research, Bangalore, 560064, India

ARTICLE INFO

Keywords:
Planar supercapacitors
Supramolecular nanofibre
Solid electrolyte
High voltage window
High scan rate

ABSTRACT

Planar microsupercapacitors are emerging as essential devices for rapid energy sourcing in on-chip circuitry. A serious limitation in comparison to planar microbatteries is the energy density that a planar supercapacitor can offer (~two orders less), which in turn relates to the maximum working potential of the electrolyte used in it, which is typically below 3 V. In this article, we report the fabrication of a planar supercapacitor with an operating voltage window, highest among the reported till date. The electrolyte used is essentially a solid in the form of nanofibres of a supramolecular donor-acceptor assembly, consisting of coronene tetracarboxylate salt (CS) and dodecyl methyl viologen (DMV), carrying positive (K^+) and negative (Br^-) ionic charges, respectively. The fibres are drop-spread across Ti microgap electrodes and the device is operated in the ambient or in a humidity-controlled cell. The device is found stable up to a working potential window of 8 V, exhibiting areal capacitance values of 0.2 mF/cm^2 under room humidity conditions (RH, 65%) which was enhanced to 9.5 mF/cm^2 under 90% RH in presence of hygroscopic KBr crystallites. The estimated areal energy and power density values are remarkable, 85 μWh cm^{-2} and 24.7 W cm^{-2} respectively. The device retained 86% capacitance even after 50000 charge-discharge cycles. Using a single device, AC line filtering is shown possible with ripple less than 5%. These extraordinary properties are borne out of the facile diffusion of ions along the 1D face-to-face arrangement of the D-A molecules in the nanofibres while the ambient oxide covered Ti surface providing the required electrochemical stability to the device.

1. Introduction

Supercapacitors as energy storage devices [1–10] are emerging in the landscape with batteries and capacitors on either sides borrowing the best of both. As capacitors, they possess high power density and cyclic stability, while targeting energy densities akin to batteries. Although there have been many results in the literature on supercapacitors with energy densities comparable to or competing with batteries [11–13], it is not yet a common sight to see supercapacitors as stand-alone devices replacing batteries. In order to increase the energy density ($\frac{1}{2}CV^2$) of a supercapacitor, most efforts in the literature focus on increasing the capacitance by enhancing the electrode surface area [14,15]. Increasing the operating voltage on the other hand, not only results in a quadratic increase in the energy density but also offers the possibility of sourcing to devices requiring high voltage operation. In this direction, efforts have been made to integrate several supercapacitors so as to achieve the desired voltage window [16]. However, it is always advantageous to stack a few high voltage supercapacitors instead of several low voltage ones. As example, the voltage of automobile batteries is typically around 12–14 V [17], which means about 12–14 1 V supercapacitors would be required. However, having them in series consumes additional space and adds to internal losses.

Thus, there is a great demand for electrolytes which offer wider voltage windows [18–21]. In case of aqueous electrolytes because of their limited electrochemical stability, the working voltage is constrained to typically 1 V, although using neutral aqueous media and suitable electrode materials, voltage windows up to 2 V have been realised [22,23]. On the other hand, organic electrolytes are usually stable up to 2.8 V [24,25] but are air-degradable, flammable, toxic and expensive. In this regard, ionic liquid based electrolytes have provided the highest reported voltage window thus far [18]. The windows range

* Corresponding author.
E-mail address: guk@cens.res.in (G.U. Kulkarni).
[1] These authors contributed equally to this work.

https://doi.org/10.1016/j.nanoen.2019.04.054
Received 19 January 2019; Received in revised form 4 April 2019; Accepted 15 April 2019
Available online 19 April 2019

up to ~4 V [26–29] but the devices lack ambient stability and suffer from low ionic conductivity [18–21]. Often, asymmetric electrode configurations are used in order to increase the voltage window [30–32]. However, asymmetric supercapacitors tend to have low cyclic stability and show oxidation/reduction peaks in the cyclic voltammogram when operated beyond the limit of the potential window of the electrolyte. These concerns are common to both volume and planar supercapacitors, though acceptable ranges of energy and power densities for the two configurations are varied [10–12]. The work reported in this article addresses the above issues with a novel planar device.

Recently, some of us reported a planar supercapacitor [33] which albeit using molecular nanofibre as electrolyte, exhibited high ambient stability (Table S1, ESI†, Supporting Information). In the present study, we have indeed realised voltage windows beyond 8 V, through a rational design of the electrolyte-electrode interface. The present device circumvents the requirement of an extra coating to protect the current collector from the harsh environment of the electrolyte. Other performance parameters such as scan rate, cyclic stability have also been examined in detail. In a demonstration, a single device could filter an 8 V AC input with ripple less than 5%.

2. Results and discussion

The present planar supercapacitor uses supramolecular 1D nanofibres as the electrolyte with Ti as the metal electrode. The nanofibres are built via self-assembly of coronene based donor (potassium salt of coronene tetracarboxylate, CS) and viologen-based acceptor (dodecyl methyl viologen, DMV) molecules (see Fig. 1a). When these donor-acceptor (D-A) molecules are co-solubilised in water, they form cylindrical micelles following surfactant-like assembly [33]. The micelles contain bilayers of charge transfer (CT) amphiphiles with hydrophobic core and hydrophilic surface. The D-A pairs are arranged radially and stacked face-to-face along the length of the nanofibre. In the nanofibre, each D and A pair contains four cations (K^+) and two anions (Br^-) respectively, where K^+ are oxygen coordinated while Br^- are solvated around the acceptor. Typical fabrication of a planar supercapacitor involves drop casting the nanofibre dispersion (0.5 mM) onto a pair of Ti electrodes separated by ~ 5 μm spacing. The device is then allowed to dry overnight in a rotary vacuum which leaves bundle of nanofibres spread across the gap (Figs. 1b and S1, ESI†). Importantly, the electrodes do not demand an additional coating (see Table S1, ESI†) as is commonly done using porous carbon [34–38] or metal oxide [39–42], avoiding an extra process step. To investigate the efficacy of the as-fabricated device, we performed cyclic voltammetry (CV) of the device in the two-electrode configuration. We performed the CV scans by gradually increasing the voltage range at a constant scan rate of 10 V/s (Fig. 1c) while ensuring capacitive nature of the curve. In the voltage window 0–1 V, the device exhibited a semi-rectangular CV curve. On gradually increasing the voltage window to 2, 4, 6 and eventually up to 8 V (see Fig. S2, ESI† for individual CV), the curve continued to be semi-rectangular, ensuring continued stability of the device. This voltage range is truly unprecedented (Table S1, ESI†); the highest values reported in the literature are less than half this range. It is this aspect which led us to carry out a systematic detailed study of the device. The origin of this extraordinary nature of the device lies in the unique combination of supramolecular nanofibre as the electrolyte and Ti as the metal electrode. Among various other metals (Au, Cu, Sn, Al, Ni), Ti was found to be extremely efficient giving rise to rectangular CV curves (Fig. S3 and Table S2, ESI†) particularly attributed to its stability in halide environment by formation of a surface TiO_2 layer in ambient (Table S3 and Fig. S4, ESI†). The sputtering deposited Ti has a very low roughness of ~2 nm (Fig. S5, ESI†), ensuring the conformal contact between 1D nanofibres and electrode.

Given the stability, we choose the 0–8 V window for further studies. Several devices were made using Ti electrodes with optimized gap of 5 μm (see Fig. S6, ESI†). The devices were tested for various scan rates as shown in Fig. 2. We began with a scan rate of 10 V/s and obtained an areal capacitance of 204 μF/cm^2 (Fig. 2a), the discharge current being 3 mA/cm^2. The scan rate was then increased to 100, 500 and 1000 V/s (Fig. 2b–d and Fig. S7, ESI†), and surprisingly, the CV loop improved. At even higher scan rates of 5000 and 10000 V/s (Fig. 2e and f), the loop was still stable though the loop shape decreased slightly. Such ultra-high scan rates are rarely found in the literature [39], most commonly used rates are below 10 V/s (Table S1, ESI†). With

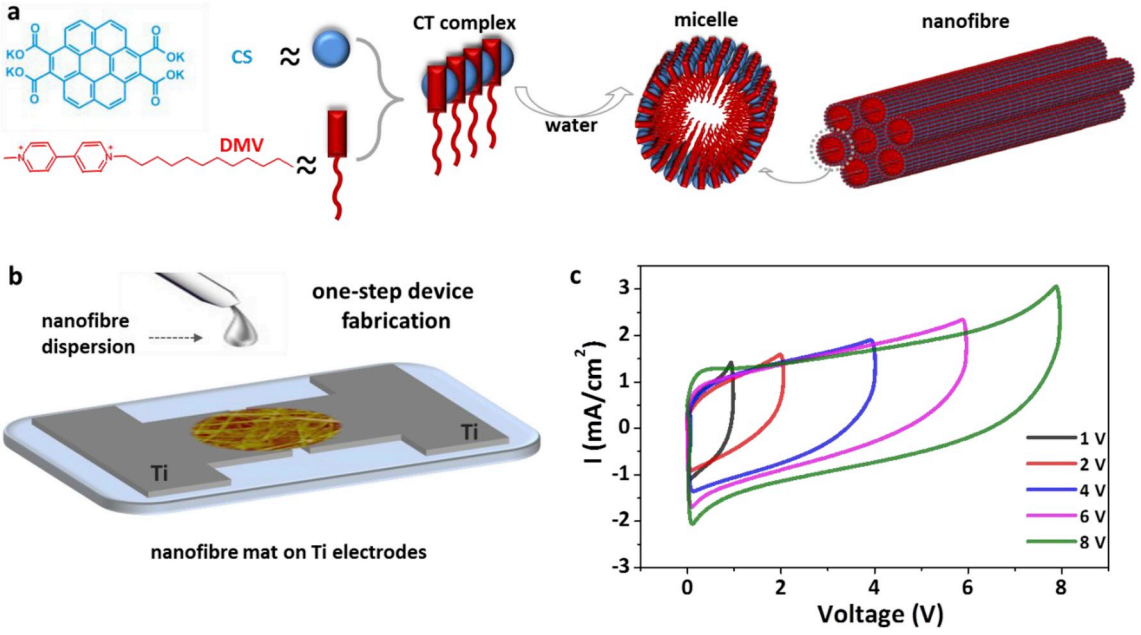

Fig. 1. (a) Structure of CS (Coronene tetracarboxylate Salt) and DMV (Dodecyl Methyl Viologen) molecules (left). Schematics of self-assembly of CS and DMV in water to form cylindrical micelle which then bundles to form nanofibre. (b) Simple fabrication of planar supercapacitor involving drop casting of nanofibre dispersion onto pre-fabricated Ti electrodes. The device was kept in vacuum evaporation for overnight to remove any residual water content on the nanofibre. An AFM image of the nanofibre mat is merged across the Ti electrodes. (c) Cyclic voltammetry of the fabricated planar supercapacitor measured at increasing voltage windows (0–1 to 0–8 V) with a scan rate of 10 V/s. No abrupt rise in current is observed even at voltage window of 0–8 V.

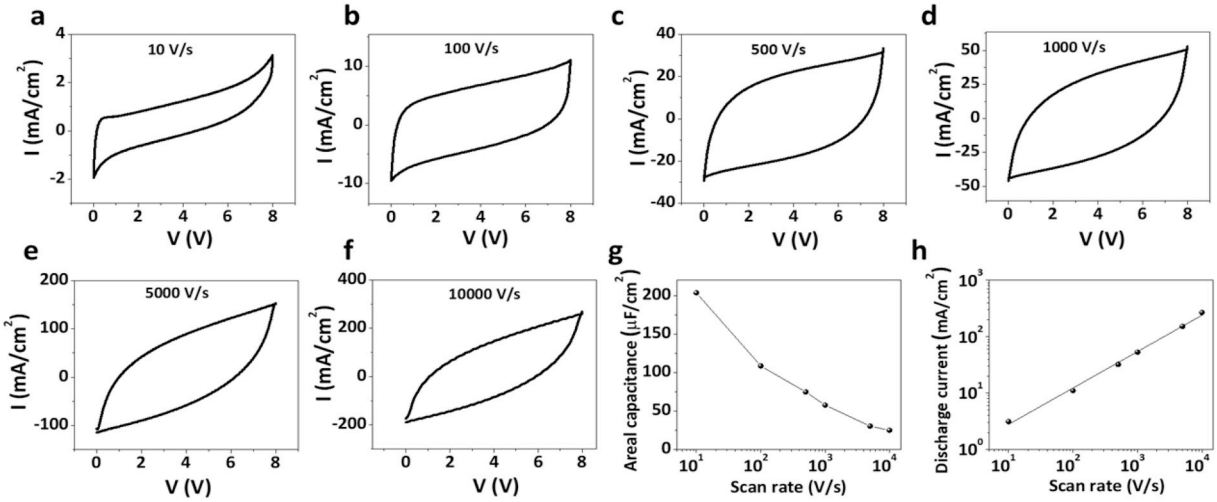

Fig. 2. (a–f) Scan rate dependent cyclic voltammetry of the device measured at voltage window of 0–8 V. Scan rates are varied from 10 V/s to 10000 V/s. Variations of (g) the areal capacitance and (h) the discharge current with the scan rate.

increasing scan rate from 10 to 10000 V/s, the discharge current increased linearly from 3 to 268 mA/cm^2 (Fig. 2h), while the areal capacitance decreased (Fig. 2g) which is rather expected. Notably in spite of increasing the scan rate by three orders (10–10000 V/s), the decrement in the areal capacitance was less than one order (from 204 to 25 μF/cm^2). We also studied the CV at lower scan rates (< 10 V/s) up to 50 mV/s (Fig. S8, ESI†). The device retains its stable performance at low scan rates as well.

Galvanostatic charge-discharge curves were measured for different current densities (Fig. 3a). The curves were semi-triangular in shape with no measurable internal resistance drop, indicating the presence of a well formed electric double layer at the electrode-electrolyte interface. Further, the capacitance retention of the device was tested taking it continuously through 50000 cycles of charge-discharge (at 8 V, 16 mA/cm^2, Fig. 3b), and the device retained nearly 86% of its initial capacitance. This electrochemical stability is comparable to other devices reported in the literature (Table S1, ESI†). The coulombic efficiency set at ~91% after 500 cycles (Fig. 3b, blue circle) and increased gradually to 97% with the charge-discharge curve becoming increasingly triangular (Fig. 3c). Similar behavior of the charge-discharge curves was also observed for a lower current density of 3 mA/cm^2 (see Fig. S9, ESI†). There was no variation observed in the morphology of the Ti electrodes and nanofibre electrolyte after 50000 charge-discharge cycles (Figs. S10 and S11 ESI†). These observations are indeed attributable to the presence of an efficient ion channel along the supramolecular nanofibres (*vide infra*).

Electrochemical impedance spectroscopy data is shown in Fig. 4. In the Nyquist plot (Fig. 4a), the variation of the imaginary part of impedance, Z″, is nearly vertical to the real part, Z′ on the x-axis, representing capacitive nature of the device. From the high-frequency region (Fig. 4a), we have estimated the equivalent series resistance and charge transfer resistance to be ~1.06 and ~8.82 Ω cm^2, respectively. In the Bode plot (Fig. 4b), the characteristic frequency (f_0) corresponding to a phase angle of −45^0 was found to be 2153 Hz, nearly four orders higher compared to a typical commercial supercapacitor (see Fig. S12, ESI†). The time constant τ_0 was calculated to be of 0.46 ms (see Fig. 4b).

As the electrical behavior of the nanofibres does depend on the relative humidity surrounding it [43], we have examined the device performance under varying relative humidity. It may be noted that the data presented above refer to ambient humidity, i.e. RH ~65%. With increasing humidity, the area under the CV curve increased, while retaining the shape as shown in Fig. 5a (also see Figs. S13 and S14, ESI†). We see that the areal capacitance increased from the ambient value, 57.63 μF/cm^2 (Fig. 2) to 360 μF/cm^2 at RH of 90% (scan rate, 1000 V/s). Working beyond 90% humidity proved difficult due to condensation, the latter being fatal to the device particularly while operating at higher voltages. Rather, we produced a hygroscopic environment around the device by sprinkling few fine grains of KBr on and around the electrodes hosting the active fibres. KBr was chosen as the hygroscopic medium as the fibre precursor itself contained K^+ and Br^- as functional entities (Fig. S15, ESI†). Indeed, the presence of the hygroscopic salt gave rise

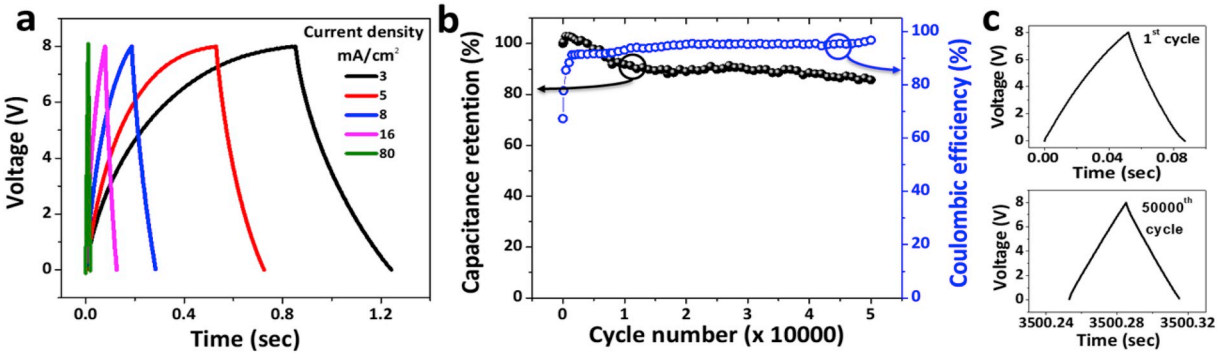

Fig. 3. (a) Galvanostatic charge-discharge curve for the device when charged to 8 V with current densities ranging from 3 to 80 mA/cm^2. (b) Capacitance retention (sphere) and coulombic efficiency (circle) of the device when subjected to repetitive charge discharge cycles for 50,000 cycles at a current density of 16 mA/cm^2 (c) CD curves for 1st and 50000th cycle.

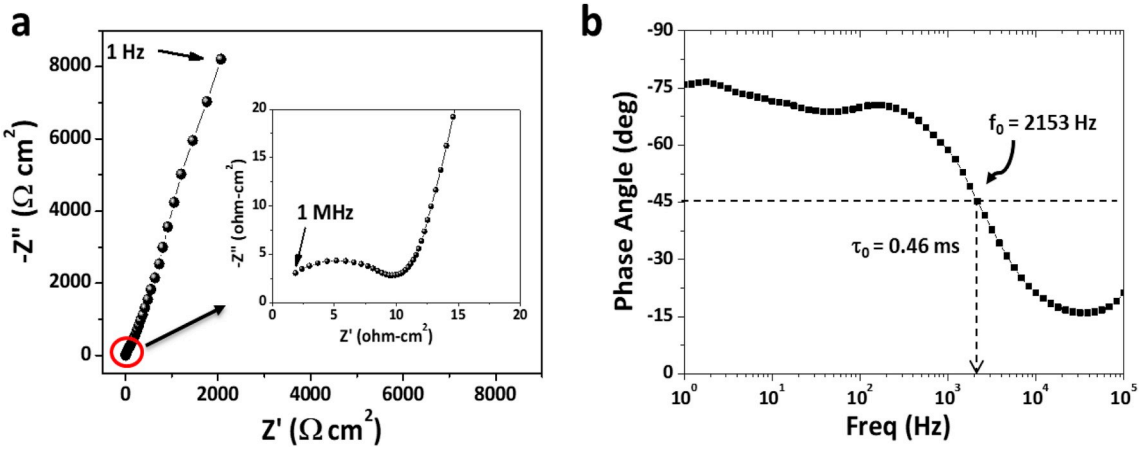

Fig. 4. Impedance analysis of the supramolecular device. (a) Nyquist plot of the supramolecular device obtained for 1 Hz to 1 MHz. Inset showing the zoom-in view for the high frequency region. (b) Bode plot: Phase angle vs frequency of the device.

to a peak performance value of 1.33 mF/cm^2 under 90% RH, other conditions remaining similar (Fig. 5b and c). For a lower scan rate of 10 V/s, the value was 9.5 mF/cm^2 (see Figs. S16, S17, and S18, ESI†). Even at low scan rates, the shape of the CV loops is virtually the same with no sign of redox peaks (see Fig. S19, ESI†).

Charge storage in CS-DMV nanofibre is intriguing considering that it can also conduct reasonably well [43]. Indeed, the nanofibre may be visualised as a core-shell-shell heterostructure as shown in Fig. S20, ESI†. The coronene-viologen D-A pairs with the characteristic π-π interaction form a conducting shell with inwardly oriented hydrocarbon chains from DMV forming the core; the latter is only a structural element in the micellar assembly and is not expected to take part either in charge storage or in conduction. There exists yet another outer dielectric shell made of methyl groups of DMV and oxygen co-ordinated K^+ (Fig. S20, ESI†). Understandably, it is this shell which may form the required thin dielectric layer for the capacitor action with K^+ from coronene and solvated Br^- from outside of the fibre as participating counterions. With K^+ held in oxygen coordination of the coronene salt, it can only contribute to orientational polarisation under an external electric field which goes well with the observed electrostatic type of behavior under dry conditions (Figs. S13 and S14, ESI†). With increasing humidity, the conduction through the D-A shell is enhanced due to tighter packing of the fibre (Fig. S21, ESI†), as revealed in the earlier studies [43]. Alongside, the ion movements in the outer shell also increase due to increased hydration (Fig. S22, ESI†), as is known in the case of crown ethers induced by the corresponding solvents [44]. In the presence of external KBr, we see enhancements in the current and capacitance values which goes well with our intuition that the KBr crystals may cause an apparent increase in the hydration level in the nanofibre neighbourhood. This notion is based on the experimental findings in the literature [45], which state that under high humid conditions, KBr crystals can host a few nm thick water layer without causing deliquescence. The latter aspect is crucial to maintain the integrity of the fibres; else any bulk condensation may dissolve away the nanofibre constituents.

The overall scenario resembles that encountered in electrolytic capacitors, with thin TiO_2 layer on Ti working as the metal oxide dielectric and nanofibres as the source of ions (see Figs. S15 and S23, ESI†). As the water molecules do not themselves take part in the transport directly, effects due to hydrolysis cannot be expected which essentially accounts for the large voltage window exhibited by the device. Thus, the system of nanofibre presented in this study is unique.

The Ragone plot of the nanofibre supercapacitor device is shown in Fig. 6 for the scan rates employed for 8 V window, along with the literature results. The trends observed with regard to the areal capacitance (Figs. 5 and S18, ESI†) also reflect in energy and power density variations (Fig. 6). Accordingly, the maximum energy and power density values obtained are 85 μWhcm^{-2} and 24.7 Wcm^{-2}, which are among the best-reported values for planar supercapacitors (see Table S4, ESI†) [35, 37, 39-41, 46-53].

AC line filtering using supercapacitors is a recent trend in the literature [54]. However, commonly available activated carbon-based devices cannot perform effective filtering because of slow response (see Fig. S12, ESI†). Often, electrodes are modified with carbon nanotubes

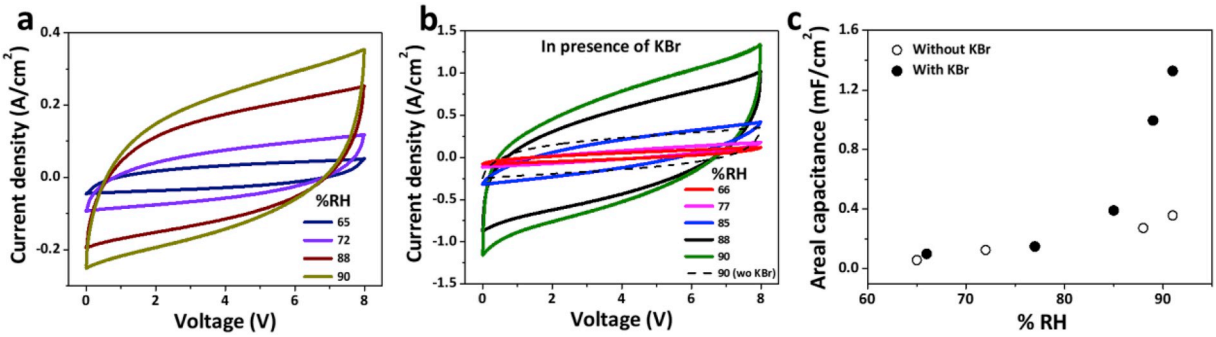

Fig. 5. Humidity dependence of the supramolecular device. (a) CV curves of the device obtained under different humidity conditions (scan rate: 1000 V/s). (b) CV curves obtained for the device in presence of KBr under different humidity conditions (scan rate: 1000 V/s). Dotted curve is the CV curve of the device measured at 90% RH without KBr and reproduced from (a). (c) Humidity dependent areal capacitance of the device (values calculated from the data in a and b) without (open circle) and with KBr (filled circle).

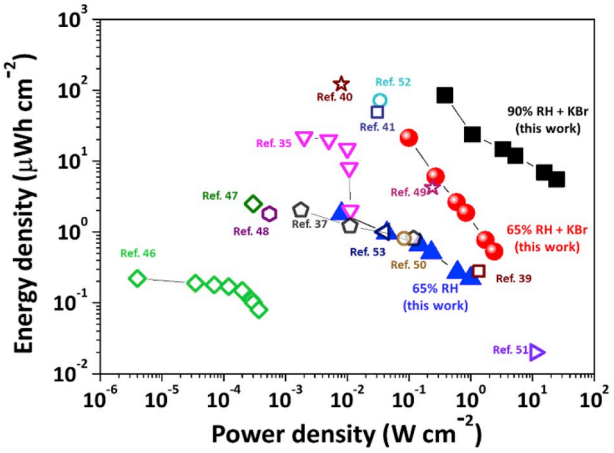

Fig. 6. Ragone plot: areal energy density vs. areal power density of the nanofibre device (filled symbols) compared with planar supercapacitor devices from the literature (open symbols), where the energy and power density values have been reported in terms of per unit area (cm^2). The values for the present device obtained at various RH are shown, 65% without (blue triangles) and with KBr sprinkling (red spheres) as well as for 90% RH in presence of KBr (black squares).

[55–57] or conducting polymers [58] for this purpose. Lower voltage window of the electrolytes is another limitation. Such supercapacitors are therefore connected in series to achieve filtering at useful voltages [59]. Here, we attempted the same using a single device. AC to DC conversion is shown in Fig. 7 using a AC filtering circuit (Fig. 7a) with our device connected as a filtering capacitor, for input line frequency of 50 Hz at 8.7 V (Fig. 7b). The pulsating DC from the bridge rectifier was smoothened to a constant DC output of 8 V (blue curve), the ripple factor being ~ 6% (see Fig. S24, ESI†). The filtering action by the nanofibre device relates to a favourable phase angle (-70^0) observed at 100 Hz (see Fig. 4b). The ripple is much less (< 5%) at higher input frequencies (Fig. 7c, d and Fig. S24, ESI†). Further, given the device configuration, one would expect it to be non-polar. Indeed, as shown in Fig. 7e, the supercapacitor could effectively filter out both positive and negative cycles.

3. Conclusions

In summary, we have demonstrated the fabrication of a planar supercapacitor with a supramolecular nanofibre system as solid electrolyte on Ti microgap electrodes. The fibre electrolyte consists of a self-assembly of donor-acceptor pairs, coronene tetracarboxylate (CS) and dodecyl methyl viologen (DMV), stabilised formed via charge transfer interactions. The device exhibited excellent stability under operating voltages up to 8 V, the highest value so far to the best of our knowledge. Increasing the humidity around the device led to a steady increase in the areal capacitance; at 90% RH, a capacitance of 360 μF/cm^2 was obtained at 1000 V/s scan rate. By introducing KBr crystallites around the device, the capacitance could be increased further to 1.33 mF/cm^2, owing to hygroscopic nature of the salt.

The device shows a very high scan rate (10000 V/s) stability, which is rare among the literature examples of supercapacitors. The device is also stable at lower scan rates (~50 mV/s). The device could work efficiently for over 50000 cycles tested in continuous charge-discharge cycles at 16 mA/cm^2 discharge current, retaining ~86% of the initial capacitance. The device showed remarkable areal energy and power density values of 85 μWhcm^{-2} and 24.7 Wcm^{-2} respectively. The excellent performance of the device (see Table S1, ESI†) owes much to the nature of the nanofibre electrolyte. The 1D arrangement of the D-A molecules in the form of a fibre seems to provide an efficient channel for the fast diffusion of K^+ and Br^- ions across the electrodes while the Ti electrode surface offers the requisite stability in halide environment. Using the device, AC voltage (8.7 V, 50 Hz to 2 kHz) filtering with less than 5% ripple was achieved. The planar supercapacitor device reported in this article may pave the way to new ideas in the design of efficient energy storage devices.

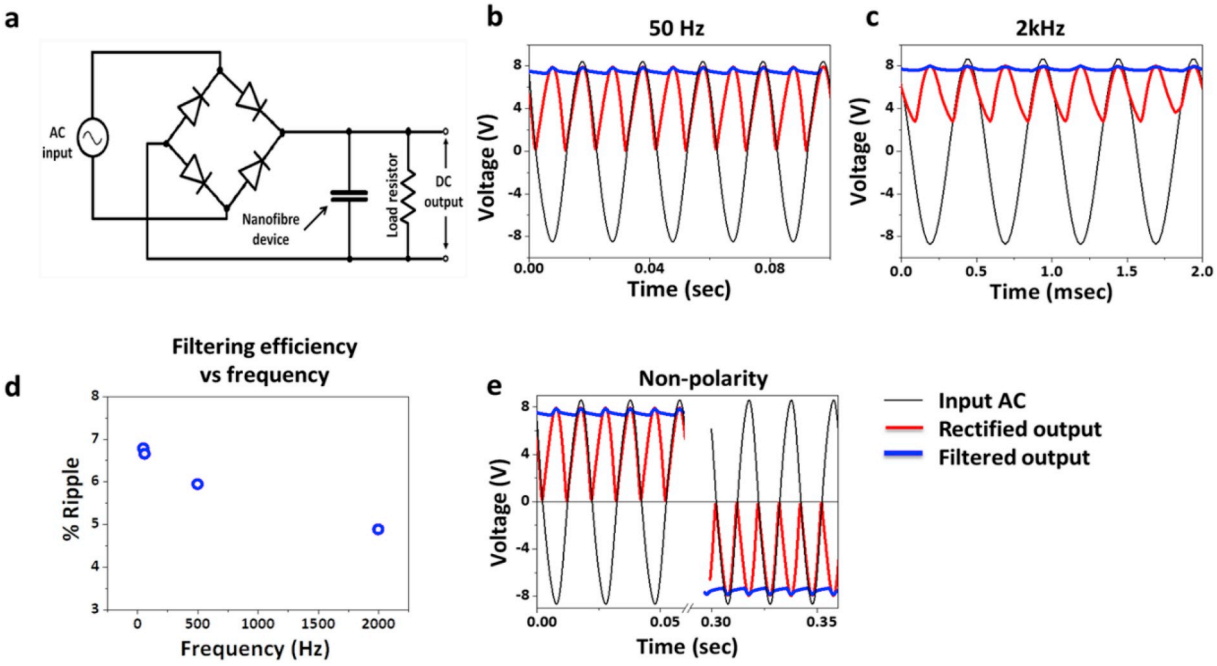

Fig. 7. AC line filtering. (a) An AC to DC filtering circuit diagram with the nanofibre device. AC line filtering with the device at input frequency (b) 50 Hz and (c) 2 kHz. (d) Filtering efficiency of the device at different frequencies. (e) Non-polarity of the nanofibre device.

4. Experimental details

4.1. Synthesis of CS-DMV electrolyte solution

The synthesis of CS-DMV electrolyte solution may be found in detail in Ref. [60]. In short, CS (coronene tetracarboxylate) was prepared by a two-fold oxidative benzogenic Diels–Alder reaction of perylene with N-ethyl maleimide and following hydrolysis with KOH in methanol. DMV (dodecyl methyl viologen) was synthesized from 4,4'-bipyridine by a controlled reaction on one nitrogen with dodecyl bromide to give mono pyridinium ion and followed by treating them with methyl iodide to amphiphilic dicationic bipyridine. The charge-transfer fibres have been assembled from injection of a methanol solution of DMV, in which the viologens are molecularly dissolved, to the aqueous solution containing free CS molecules (10% v/v methanol in water). Further, the concentration of the CS-DMV nanofibre electrolyte solution has been varied by adding an appropriate amount of deionized water.

4.2. Device fabrication

For the fabrication of the planar supercapacitor, the glass substrates were cleaned in piranha solution followed by washing with acetone, IPA and distilled water. A carbon fibre of 6 µm diameter was then attached firmly on the glass substrate to serve as a shadow mask for Ti electrode deposition by sputtering (Model No. BT300, HHV, India). After removing the mask, a 1 µL solution of CS-DMV supramolecular electrolyte solution was drop cast on to the gap and kept overnight in vacuum desiccator. Other metal electrodes (Au, Ni, Sn, Al, Cu) were prepared by the thermal evaporation method (VEC solutions, India).

4.3. Characterization

The electrochemical measurements were performed in the two-electrode configuration using CH Instruments 660 E (Austin, TX, USA) after making silver paste contact with the metallic electrodes. The morphology of the nanofibres was examined using a scanning electron microscope (Nova NanoSEM 600 instrument, FEI Co., The Netherlands), and energy dispersive spectroscopic (EDS) mapping was done by EDAX Genesis V4.52 (USA) attached to the SEM column. AFM measurements were carried out using Multimode, Veeco digital instruments, USA with Nanoscope IV controller. AC signal filtering measurements were performed using Tektronix MDO4054C oscilloscope.

4.4. RH variation

A cell was made for varying the RH and switching between two RH levels was done using a Tee with an N_2 flow rate of 200–300 sccm connected to a flask containing water. A commercial humidity meter, Testo 410–2, was used to measure the obtained RH.

4.5. Calculations

The areal capacitance values (C_A) of the device were calculated from the cyclic voltammetry data according to the following equation:

$$C_A = A_{CV} / (V*S*A_d) \quad (1)$$

where, A_{CV} = integrated area of the CV plot, V = potential window, S = scan rate, A_d = active area of the device, corresponding to the gap area.

The energy density (E_d) of the device was obtained from the following equation

$$E_d = ½ \times C_A \times V^2/3600 \quad (2)$$

The power density (P_d) of the device was calculated from the following equation

$$P_d = (E_d/\Delta t) \times 3600 \quad (3)$$

where, Δt is the discharge time in seconds.

Acknowledgements

We acknowledge Prof. C. N. R. Rao as a constant source of inspiration. We acknowledge Nano Mission, Department of Science and Technology, India for funding. The authors thank Shikha Dhiman for providing the molecules. S.K. thanks Aman Anand and Bharath B. for assisting in fabrication of electrodes, and Chaitali Sow for helping with FESEM measurements. U.M. thanks IGSTC for the fellowship.

Appendix A. Supplementary data

Supplementary data to this article can be found online at https://doi.org/10.1016/j.nanoen.2019.04.054.

References

[1] P. Simon, Y. Gogotsi, Materials for electrochemical capacitors, Nat. Mater. 7 (2008) 845–854 https://doi.org/10.1038/nmat2297.
[2] G. Wang, L. Zhang, J. Zhang, A review of electrode materials for electrochemical supercapacitors, Chem. Soc. Rev. 41 (2012) 797–828 https://doi.org/10.1039/c1cs15060j.
[3] P. Simon, Y. Gogotsi, B. Dunn, Where do batteries end and supercapacitors begin? Science 343 (2014) 1210–1211 https://doi.org/10.1126/science.1249625.
[4] Y. Gogotsi, P. Simon, True performance metrics in electrochemical energy storage, Science 334 (2011) [917]–[918] https://doi.org/10.1126/science.1213003.
[5] R. Kötz, M. Carlen, Principles and applications of electrochemical capacitors, Electrochim. Acta 45 (2000) 2483–2498 https://doi.org/10.1016/S0013-4686(00)00354-6.
[6] M. Winter, R.J. Brodd, What are batteries, fuel cells, and supercapacitors? Chem. Rev. 104 (2004) 4245–4269 https://doi.org/10.1021/cr020730k.
[7] J.G. Koomey, H.S. Matthews, E. Williams, Smart everything: will intelligent systems reduce resource use? Annu. Rev. Environ. Resour. 38 (2013) 311–343 https://doi.org/10.1146/annurev-environ-021512-110549.
[8] M. Vangari, T. Pryor, L. Jiang, Supercapacitors: review of materials and fabrication methods, J. Energy Eng. 139 (2013) 72–79 https://doi.org/10.1061/(ASCE)EY.1943-7897.0000102.
[9] A. González, E. Goikolea, J.A. Barrena, R. Mysyk, Review on supercapacitors: technologies and materials, Renew. Sustain. Energy Rev. 58 (2016) 1189–1206 https://doi.org/10.1016/j.rser.2015.12.249.
[10] H. Chen, T.N. Cong, W. Yang, C. Tan, Y. Li, Y. Ding, Progress in electrical energy storage system: a critical review, Prog. Nat. Sci-Mater. 19 (2009) 291–312 https://doi.org/10.1016/j.pnsc.2008.07.014.
[11] N.A. Kyeremateng, T. Brousse, D. Pech, Microsupercapacitors as miniaturized energy-storage components for on-chip electronics, Nat. Nanotechnol. 12 (2016) 7–15 https://doi.org/10.1038/NNANO.2016.196.
[12] M. Beidaghi, Y. Gogotsi, Capacitive energy storage in micro-scale devices: recent advances in design and fabrication of microsupercapacitors, Energy Environ. Sci. 7 (2014) [867]–[884] https://doi.org/10.1039/c3ee43526a.
[13] M.F. El-Kady, M. Ihns, M. Li, J.Y. Hwang, M.F. Mousavi, L. Chaney, A.T. Lech, R.B. Kaner, Engineering three-dimensional hybrid supercapacitors and microsupercapacitors for high-performance integrated energy storage, Proc. Natl. Acad. Sci. U.S.A. 112 (2015) 4233–4238 https://doi.org/10.1073/pnas.1420398112.
[14] a) Y. Zhang, H. Feng, X. Wu, L. Wang, A. Zhang, T. Xia, H. Dong, X. Li, L. Zhang, Progress of electrochemical capacitor electrode materials: a review, Int. J. Hydrog. Energy. 34 (2009) 4889–4899 https://doi.org/10.1016/j.ijhydene.2009.04.005;
b) Y. Jun, W. Qian, W. Tong, F. Zhuangjun, Recent advances in design and fabrication of electrochemical supercapacitors with high energy densities, Adv. Energy Mater. 4 (2014) 1300816 https://doi.org/10.1002/aenm.201300816.
[15] a) M. Zhi, C. Xiang, J. Li, M. Li, N. Wu, Nanostructured carbon–metal oxide composite electrodes for supercapacitors: a review, Nanoscale 5 (2013) 72–88 https://doi.org/10.1039/c2nr32040a;
b) C. Liu, Z. Yu, D. Neff, A. Zhamu, B.Z. Jang, Graphene-based supercapacitor with an ultrahigh energy density, Nano Lett. 10 (2010) 4863–4868 https://doi.org/10.1021/nl102661q.
[16] a) S. Hao, F. Xuemei, X. Songlin, J. Yishu, P. Huisheng, Electrochemical capacitors with high output voltages that mimic electric eels, Adv. Mater. 28 (2016) 2070–2076 https://doi.org/10.1002/adma.201505742;
b) X. Li, Y. Cui, M. Qi, H. Wu, Y. Xie, X. Zang, D. Wen, K.S. Teh, J. Ye, Z. Zhou, Q.A. Huang, W. Cai, L. Lin, A 1000-volt planar micro-supercapacitor by direct-write laser engraving of polymers, IEEE 30th International Conference on Micro Electro

Mechanical Systems (MEMS) 2017, 2017, p. 821 https://doi.org/10.1109/MEMSYS.2017.7863534.
[17] H. Budde-Meiwes, J. Drillkens, B. Lunz, J. Muennix, S. Rothgang, J. Kowal, D.U. Sauer, A review of current automotive battery technology and future prospects, Proc. Inst. Mech. Eng. D J. Automob. Eng. 227 (2013) 761–776 https://doi.org/10.1177/0954407013485567.
[18] C. Zhong, Y. Deng, W. Hu, J. Qiao, L. Zhang, J. Zhang, A review of electrolyte materials and compositions for electrochemical supercapacitors, Chem. Soc. Rev. 44 (2015) 7484–7539 https://doi.org/10.1039/c5cs00303b.
[19] H. Gao, K. Lian, Proton-conducting polymer electrolytes and their applications in solid supercapacitors: a review, RSC Adv. 4 (2014) 33091–33113 https://doi.org/10.1039/C4RA05151C.
[20] S. Pohlmann, R.-S. Kühnel, T.A. Centeno, A. Balducci, The influence of anion–cation combinations on the physicochemical properties of advanced electrolytes for supercapacitors and the capacitance of activated carbons, ChemElectroChem 1 (2014) 1301–1311 https://doi.org/10.1002/celc.201402091.
[21] P. Simon, Y. Gogotsi, Capacitive energy storage in nanostructured carbon-electrolyte systems, Acc. Chem. Res. 46 (2013) 1094–1103 https://doi.org/10.1021/ar200306b.
[22] K. Fic, G. Lota, M. Meller, E. Frackowiak, Novel insight into neutral medium as electrolyte for high-voltage supercapacitors, Energy Environ. Sci. 5 (2012) 5842–5850 https://doi.org/10.1039/C1EE02262H.
[23] M.P. Bichat, E. Raymundo-Piñero, F. Béguin, High voltage supercapacitor built with seaweed carbons in neutral aqueous electrolyte, Carbon 48 (2010) 4351–4361 https://doi.org/10.1016/j.carbon.2010.07.049.
[24] E. Kovalska, C. Kocabas, Organic electrolytes for graphene-based supercapacitor: liquid, gel or solid, Mater, Today Commun 7 (2016) 155–160 https://doi.org/10.1016/j.mtcomm.2016.04.013.
[25] Y. Liang, F. Liang, H. Zhong, Z. Li, R. Fu, D. Wu, An advanced carbonaceous porous network for high-performance organic electrolyte supercapacitors, J. Mater. Chem. 1 (2013) 7000–7005 https://doi.org/10.1039/C3TA11051F.
[26] K.L.V. Aken, M. Beidaghi, Y. Gogotsi, Formulation of ionic-liquid electrolyte to expand the voltage window of supercapacitors, Angew. Chem. Int. Ed. 54 (2015) 4806–4809 https://doi.org/10.1002/anie.201412257.
[27] M. Armand, F. Endres, D.R. MacFarlane, H. Ohno, B. Scrosati, Ionic-liquid materials for the electrochemical challenges of the future, Nat. Mater. 8 (2009) 621–629 https://doi.org/10.1038/nmat2448.
[28] A. Balducci, R. Dugas, P.L. Taberna, P. Simon, D. Plée, M. Mastragostino, S. Passerini, High temperature carbon–carbon supercapacitor using ionic liquid as electrolyte, J. Power Sources 165 (2007) 922–927 https://doi.org/10.1016/j.jpowsour.2006.12.048.
[29] D.R. MacFarlane, N. Tachikawa, M. Forsyth, J.M. Pringle, P.C. Howlett, G.D. Elliott, J.H. Davis, M. Watanabe, P. Simon, C.A. Angell, Energy applications of ionic liquids, Energy Environ. Sci. 7 (2014) 232–250 https://doi.org/10.1039/C3EE42099J.
[30] C. Nitin, L. Chao, M. Julian, N. Narasimha, Z. Lei, J. Yeonwoong, T. Jayan, Asymmetric supercapacitor electrodes and devices, Adv. Mater. 29 (2017) 1605336 https://doi.org/10.1002/adma.201605336.
[31] V. Khomenko, E. Raymundo-Pinero, E. Frackowiak, F. Beguin, High-voltage asymmetric supercapacitors operating in aqueous electrolyte, Appl. Phys. A Mater. Sci. Processr. 82 (2006) 567–573 https://doi.org/10.1007/s00339-005-3397-8.
[32] F. Zhuangjun, Y. Jun, W. Tong, Z. Linjie, N. Guoqing, L. Tianyou, W. Fei, Asymmetric supercapacitors based on graphene/MnO_2 and activated carbon nanofiber electrodes with high power and energy density, Adv. Funct. Mater. 21 (2011) 2366–2375 https://doi.org/10.1002/adfm.201100058.
[33] U. Mogera, M. Gedda, S.J. George, G.U. Kulkarni, Supramolecular nanofibres as ambient stable wide voltage window electrolyte for micro-supercapacitors, ChemNanoMat 3 (2017) 39–43 https://doi.org/10.1002/cnma.201600319.
[34] J. Lin, C. Zhang, Z. Yan, Y. Zhu, Z. Peng, R.H. Hauge, D. Natelson, J.M. Tour, 3-dimensional graphene carbon nanotube carpet-based microsupercapacitors with high electrochemical performance, Nano Lett. 13 (2013) 72–78 https://doi.org/10.1021/nl3034976.
[35] D. Pech, M. Brunet, H. Durou, P. Huang, V. Mochalin, Y. Gogotsi, P.L. Taberna, P. Simon, Ultrahigh-power micrometre-sized supercapacitors based on onion-like carbon, Nat. Nanotechnol. 5 (2010) 651–654 https://doi.org/10.1038/nnano.2010.162.
[36] W. Gao, N. Singh, L. Song, Z. Liu, A.L.M. Reddy, L. Ci, R. Vajtai, Q. Zhang, B. Wei, P.M. Ajayan, Direct laser writing of micro-supercapacitors on hydrated graphite oxide films, Nat. Nanotechnol. 6 (2011) 496–500 https://doi.org/10.1038/nnano.2011.110.
[37] M.F. El-Kady, R.B. Kaner, Scalable fabrication of high-power graphene micro-supercapacitors for flexible and on-chip energy storage, Nat. Commun. 4 (2013) 1475 https://doi.org/10.1038/ncomms2446.
[38] C. Shen, X. Wang, S. Li, J. g. Wang, W. Zhang, F. Kang, A high-energy-density micro supercapacitor of asymmetric MnO_2 – carbon configuration by using micro-fabrication technologies, J. Power Sources 234 (2013) 302–309 https://doi.org/10.1016/j.jpowsour.2012.10.101.
[39] T.M. Dinh, K. Armstrong, D. Guay, D. Pech, High-resolution on-chip supercapacitors with ultra-high scan rate ability, J. Mater. Chem. 2 (2014) 7170–7174 https://doi.org/10.1039/C4TA00640B.
[40] A. Ferris, S. Garbarino, D. Guay, D. Pech, 3D RuO_2 microsupercapacitors with remarkable areal energy, Adv. Mater. 27 (2015) 6625–6629 https://doi.org/10.1002/adma.201503054.
[41] T.M. Dinh, A. Achour, S. Vizireanu, G. Dinescu, L. Nistor, K. Armstrong, D. Guay, D. Pech, Hydrous RuO_2/carbon nanowalls hierarchical structures for all-solid-state ultrahigh-energy-density micro-supercapacitors, Nanomater. Energy 10 (2014) 288–294 https://doi.org/10.1016/j.nanoen.2014.10.003.
[42] G. Lee, D. Kim, D. Kim, S. Oh, J. Yun, J. Kim, S.-S. Lee, J.S. Ha, Stretchable and patchable array of high performance microsupercapacitors using non-aqueous solvent based gel electrolyte, Energy Environ. Sci. 8 (2015) 1764–1774 https://doi.org/10.1039/C5EE00670H.
[43] a) U. Mogera, A.A. Sagade, S.J. George, G.U. Kulkarni, Ultrafast response humidity sensor using supramolecular nanofibre and its application in monitoring breath humidity and flow, Sci. Rep. 4 (2014) 4103 https://doi.org/10.1038/srep04103;
b) A. Bhattacharyya, M.K. Sanyal, U. Mogera, S.J. George, M.K. Mukhopadhyay, S. Maiti, G.U. Kulkarni, In-situ GISAXS study of supramolecular nanofibers having ultrafast humidity sensitivity, Sci. Rep. 7 (2017) 246 https://doi.org/10.1038/s41598-017-00309-2.
[44] a) G.W. Gokel, W.M. Leevy, M.E. Weber, Crown ethers: sensors for ions and molecular scaffolds for materials and biological models, Chem. Rev. 104 (2004) 2723–2750 https://doi.org/10.1021/cr020080k;
b) J.W. Steed, J.L. Atwood, Supramolecular Chemistry, second ed., John Wiley & Sons Ltd, 2009.
[45] a) K. Arima, P. Jiang, X. Deng, H. Bluhm, M. Salmeron, Water adsorption, solvation, and deliquescence of potassium bromide thin films on SiO2 studied by ambient-pressure x-ray photoelectron spectroscopy, J. Phys. Chem. C 114 (2010) 14900–14906 https://doi.org/10.1021/jp101683z;
b) R. Rai, Triloki, N. Ghosh, B.K. Singh, Effect of humid air exposure on photoemissive and structural properties of KBr thin film photocathode, Nucl. Instrum. Methods Phys. Res. 787 (2015) 125–129 https://doi.org/10.1016/j.nima.2014.11.073;
c) M. Luna, F. Rieutord, N.A. Melman, Q. Dai, M. Salmeron, Adsorption of water on alkali halide surfaces studied by scanning polarization force microscopy, J. Phys. Chem. A 102 (1998) 6793–6800 https://doi.org/10.1021/jp9820875.
[46] Y. Shao, J. Li, Y. Li, H. Wang, Q. Zhang, R.B. Kaner, Flexible quasi-solid-state planar micro-supercapacitor based on cellular graphene films, Mater. Horiz. 4 (2017) 1145–1150 https://doi.org/10.1039/C7MH00441A.
[47] H. Xiao, Z.S. Wu, L. Chen, F. Zhou, S. Zheng, W. Ren, H.-M. Cheng, X. Bao, One step device fabrication of phosphorene and graphene interdigital micro-supercapacitors with high energy density, ACS Nano 11 (2017) 7284–7292 https://doi.org/10.1021/acsnano.7b03288.
[48] B. Xie, Y. Wang, W. Lai, W. Lin, Z. Lin, Z. Zhang, P. Zou, Y. Xu, S. Zhou, C. Yang, F. Kang, C.P. Wong, Laser-processed graphene based micro-supercapacitors for ultrathin, rollable, compact and designable energy storage components, Nanomater. Energy 26 (2016) [276]–[285] https://doi.org/10.1016/j.nanoen.2016.04.045.
[49] P. Huang, D. Pech, R. Lin, J.K. McDonough, M. Brunet, P.L. Taberna, Y. Gogotsi, P. Simon, On-chip micro-supercapacitors for operation in a wide temperature range, Electrochem. Commun. 36 (2013) 53–56 https://doi.org/10.1016/j.elecom.2013.09.003.
[50] P. Huang, M. Heon, D. Pech, M. Brunet, P.L. Taberna, Y. Gogotsi, S. Lofland, J.D. Hettinger, P. Simon, Micro-supercapacitors from carbide derived carbon (CDC) films on silicon chips, J. Power Sources 225 (2013) 240–244 https://doi.org/10.1016/j.jpowsour.2012.10.020.
[51] D. Pech, M. Brunet, T.M. Dinh, K. Armstrong, J. Gaudet, D. Guay, Influence of the configuration in planar interdigitated electrochemical micro-capacitors, J. Power Sources 230 (2013) 230–235 https://doi.org/10.1016/j.jpowsour.2012.12.039.
[52] H. Durou, D. Pech, D. Colin, P. Simon, P.L. Taberna, M. Brunet, Wafer-level fabrication process for fully encapsulated micro-supercapacitors with high specific energy, Microsyst. Technol. 18 (2012) 467–473 https://doi.org/10.1007/s00542-011-1415-7.
[53] S. Zheng, Z. Li, Z.S. Wu, Y. Dong, F. Zhou, S. Wang, Q. Fu, C. Sun, L. Guo, X. Bao, High packing density unidirectional arrays of vertically aligned graphene with enhanced areal capacitance for high-power micro- supercapacitors, ACS Nano 11 (2017) 4009–4016 https://doi.org/10.1021/acsnano.7b00553.
[54] Z. Fan, N. Islam, S.B. Bayne, Towards kilohertz electrochemical capacitors for filtering and pulse energy harvesting, Nanomater. Energy 39 (2017) 306–320 https://doi.org/10.1016/j.nanoen.2017.06.048.
[55] Y. Yoo, S. Kim, B. Kim, W. Kim, 2.5 V compact supercapacitors based on ultrathin carbon nanotube films for AC line filtering, J. Mater. Chem. 3 (2015) 11801–11806 https://doi.org/10.1039/C5TA02073E.
[56] Y.J. Kang, Y. Yoo, W. Kim, 3-V solid-state flexible supercapacitors with ionic-liquid-based polymer gel electrolyte for AC line filtering, ACS Appl. Mater. Interfaces 8 (2016) 13909–13917 https://doi.org/10.1021/acsami.6b02690.
[57] Y. Rangom, X. Tang, L.F. Nazar, Carbon nanotube-based supercapacitors with excellent ac line filtering and rate capability via improved interfacial impedance, ACS Nano 9 (2015) 7248–7255 https://doi.org/10.1021/acsnano.5b02075.
[58] N. Kurra, M.K. Hota, H.N. Alshareef, Conducting polymer micro-supercapacitors for flexible energy storage and AC line-filtering, Nanomater. Energy 13 (2015) 500–508 https://doi.org/10.1016/j.nanoen.2015.03.018.
[59] Y. Yoo, J. Park, M.-S. Kim, W. Kim, Development of 2.8 V Ketjen black supercapacitors with high rate capabilities for AC line filtering, J. Power Sources 360 (2017) 383–390 https://doi.org/10.1016/j.jpowsour.2017.06.032.
[60] K.V. Rao, K. Jayaramulu, T.K. Maji, S.J. George, Supramolecular hydrogels and high-aspect-ratio nanofibers through charge-transfer-induced alternate coassembly, Angew Chem. Int. Ed. Engl. 49 (2010) 4218–4222 https://doi.org/10.1002/anie.201000527.

Suman Kundu is a PhD student at Centre for Nano and Soft Matter Sciences (CeNS), Bangalore under the supervision of Prof. Giridhar U. Kulkarni since July 2015. He received his Bachelor's Degree in 2012 from St. Xavier's College, Kolkata and Master's Degree in 2014 from Indian Institute of Technology (Indian School of Mines), Dhanbad. His research interests focus on supramolecules and graphene based materials for the applications in electrochemical energy storage and gas sensing

Dr. Umesh Mogera received his Ph.D. at Jawaharlal Nehru Centre for Advanced Scientific Research, Bangalore in 2016. During his Ph.D., he worked on supramolecular based 1D nanofibre based devices and graphene. He later joined Centre for Nano and Soft Matter Sciences, Bangalore as a postdoctoral fellow where he worked on a twisted graphene system. He is currently continuing his postdoctoral studies at the University of California, Los Angeles

Prof. Subi George is currently leading a supramoelcular chemistry group at the New Chemistry Unit of JNCASR, Jawaharlal Nehru Centre for Advanced Scientific Research (JNCASR), Bangalore, India. He has obtained his PhD degree at the National Institute for Interdisciplinary Science and Technology, India in 2004 and during 2005–2008, he has been a post-doctoral fellow at the Eindhoven University of Technology, The Netherlands. His current research interests focus on Functional Supramolecular Polymers, Living and Non-equilibrium supramolecular polymerization, Supramolecular Chirality and Organic-inorganic hybrid assemblies. In 2019, he has been elected as the Fellow of Indian Academy of Sciences

Prof. Giridhar U. Kulkarni is the Director of Centre for Nano and Soft Matter Sciences (CeNS), Bangalore and is a Professor at Jawaharlal Nehru Centre for Advance Scientific Research. He received his PhD from Indian Institute of Science in 1992. He has held visiting or adjunct positions at Cardiff, Tokyo and Purdue universities, TASC INFM-Trieste, Scuola Normale Superiore – Pisa and so on. His research interests are focused on new strategies in synthesis of nanomaterials, nanopatterning and nanodevice fabrication including of molecular systems. He is a Fellow of National Academy of Sciences, Indian Academy of Sciences and Asia Pacific Academy of Materials